

*Article*

# Experiment Investigation and Optimization for Slider Bonding Process to Enhance the Shear Strength of Epoxy Adhesive Joint

Santi Pumkrachang<sup>1</sup>, Krisada Asawarungsaengkul<sup>2,\*</sup>, and Parames Chutima<sup>3</sup>

<sup>1</sup> Department of Industrial Engineering, Faculty of Engineering, King Mongkut's University of Technology North Bangkok, Bangkok 10800, Thailand

<sup>2</sup> Operations Research and Engineering Management Research Center, Department of Industrial Engineering, Faculty of Engineering, King Mongkut's University of Technology North Bangkok, Bangkok 10800, Thailand

<sup>3</sup> Department of Industrial Engineering, Faculty of Engineering, Chulalongkorn University, Bangkok 10300, Thailand

\*E-mail: krisada.a@eng.kmutnb.ac.th (Corresponding author)

**Abstract.** The shear strength of adhesive bonding between the slider and suspension greatly affects the quality of the hard disk drive. Therefore, this paper intends to determine the optimal slider bonding parameters which can maximize the shear strength of the adhesive joint. The response surface methodology (RSM) and optimization are employed to investigate the effects of five process parameters to the shear strength of the adhesive joint. Next, the central composite design which is a RSM is conducted. The analysis of variance is used to identify the significant terms of the quadratic regression model. Then, the optimization approach is utilized to determine the optimal process parameters with the mean shear strength of 257.62 gf. The confirmation experiment to validate the quadratic model reveals that the prediction error is only 1.6% which is acceptable. Next, the regression model is also used to define the optimal process conditions under the capacity constraint. In this case, the regression model can provide the accurate prediction of the shear strength with 1.14% error. In conclusion, the RSM and optimization approach can effectively yield the optimal process parameters that can enhance the shear strength of the adhesive joint to achieve the appropriate quality level.

**Keywords:** Slider bonding, shear strength, adhesive joint, response surface methodology, optimization.

**ENGINEERING JOURNAL** Volume 25 Issue 9

Received 20 May 2021

Accepted 28 August 2021

Published 30 September 2021

Online at <https://engj.org/>

DOI:10.4186/ej.2021.25.9.33

## 1. Introduction

Hard disk drive (HDD) is a data storage device in which required for every system that intends to store and retrieving digital information. The market demand for HDD devices is exceptionally strong due to the data-centric era. The data or information are flowed and stored throughout the supply chain. Although the actual unit shipment of HDD might get impact form the instability of global economy, however market demand of the past decade constantly beyond 500 million units annually. Strong market demand stimulates the HDD industry to become one of the most active industries in the present day.

Read and write head of the HDD so call slider is an important component used for reading and writing magnetic signal from/to the magnetic disk, then perform the signal processing. Slider is attached to the bonding pad on suspension via slider bonding process and proceeded to a few process steps. The finish goods of this process is the head gimbal assembly (HGA). HGA flies over the magnetic disk at the rotational speed of at least 5400 rpm with the gap between the slider and magnetic disk less than 20 nanometer. The narrow flying gap can generate high shear force on the HGA surface that facing to the magnetic disk. Thus, the adhesive strength of the slider adhesion is important to prevent the slider from falling off during the operation in the HDD. Therefore, one of the key process output variables (KPOVs) of HGA is the adhesive bonding strength. This paper is organized by following the analyze, improve, and control phases of the six sigma approach. A major outcome after improve phase is the empirical model which shows the effects of key process input variables (KPIVs) to the key process output variable.

HGA consists of two important components which are the slider head and 20  $\mu\text{m}$  thick steel suspension displayed in Fig. 1(a) and Fig. 1(b). The slider is made of aluminum titanium carbide (AlTiC); while suspension pad is made of stainless steel coated by gold. The dimension of slider is 750x850x280  $\mu\text{m}$ . The slider is attached onto the suspension by the amount of less than 10 nanoliter of epoxy resin and then fully cure by UV beam and IR oven. The adhesive used in this HGA product is dual curable epoxy. The amount of epoxy adhesive is limited by the footprint of the suspension as in Fig. 1(a). In order to gain high HDD capacity, the size of slider and suspension are continuously reduced. Thus, this small size of slider potentially affects to the shear strength of adhesive joint and to the reliability of HGA. For the process control purpose, the process parameters as KPIVs must be optimized and recorded into the control plan. In slider bonding process, some process parameters for instant adhesive amount and curing time etc. are the critical factors contribute to the adhesive shear strength.

The adhesive has been used in various assembly process to join two parts together. The shear strength is a major quality characteristic of the adhesive joint. The study on the shear test method, the failure modes,

adhesive types, process conditions, and mechanical properties for the adhesive joint can be found in [1-12]. The adhesive for joining wood to wood and the effects of conditioning treatment processes to the shear strength of adhesive joint was done by [1]. The effects of the process conditions such as surface treatment, adhesive thickness, additive materials were presented in [2-5]. The common test equipment for adhesive shear test is the standard tensile test equipment as in [1-7, 11, 12]. The shear test method of adhesive joint for HGA was internally developed by adopting the die shear test concept. The shear test which applies force through shear tool to the component can be found in [8-10, 13, 14]. It is noticed that the electronic assembly performed the shear test by applying force to the assembly component. Other papers studied fatigue damage, and failure behavior of adhesive bonding were done by [6, 7]. The reliability of the adhesive joint under various conditions were studied by [8, 9, 13]. The force-displacement curves were depicted in these papers. This curve was used to reflect the quality of the adhesive joint.

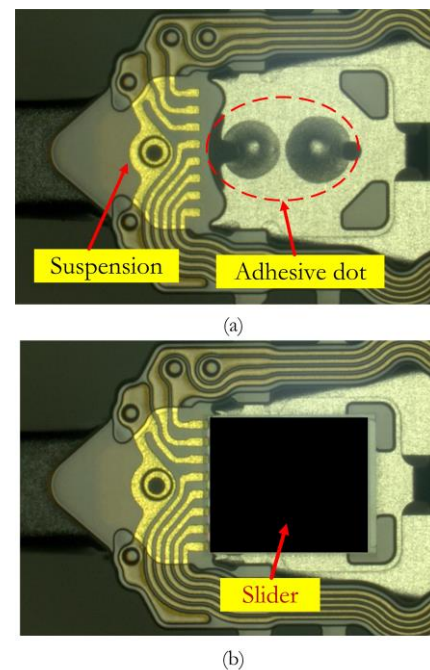


Fig. 1. (a) Epoxy adhesive dot on the suspension (b) Slider placed on the suspension pad.

Typically, the adhesive was used to perform both similar and dissimilar joints. For HGA, the epoxy adhesive is used to joint two dissimilar materials. This paper focuses on the investigation of the optimal process conditions to improve the shear strength. Design of experiment (DOE) and statistical analysis have been used to determine the key process input variables which highly contributes to the change of KPOV. The DOE and regression analysis were utilized to determine the optimal process conditions [15-24]. The regression model can be obtained by the mathematical operation based on the data from the DOE plan. The factorial experiment design can yield the first order regression model while the response surface

methodology can be utilized to formulate the second order regression model. The analysis of variance (ANOVA) and regression analysis was used to formulate the relationship between the percentage of aluminium by weight and the particle sizes in epoxy aluminium composite to the flexural modulus [15]. This regression model can be solved to obtain the optimal predictors. The effect of bonding parameters to the adhesive strength of T-joint was investigated by the general full factorial design [16]. A study of the effect of the process parameters to the interfacial strength of the epoxy resin composites was discussed in [17]. The ANOVA has been utilized to determine the significant factors for the factorial design. Moreover, the factorial plots were used to observe the optimal process conditions for the general full factorial design as in [16, 17]. Another DOE technique which is Taguchi method was applied to optimize the welding process parameters [18].

The second order or quadratic regression model can be used when the nonlinear model is required. Response surface methodology is an experiment design used to formulate the second order regression model. The application of RSM in process optimization can be found in [19-25]. After the regression model is obtained, the optimization approach is then utilized to determine the best condition for the process control. The central composite design (CCD) as a RSM was employed to optimize the thermal mechanical properties of a novel flip chip [19]. The multi-criteria optimization was applied to determine the optimal design of the flip chip technology. Optimization of biodiesel production using RSM was done by [20]. Experiment investigations using RSM for process optimization of the strength of adhesive joint were proposed by [21, 22, 24, 25]. Some parameters such as material parameters, ductile adhesive volume fraction, overlap, adhesive thickness, etc. were the input variables for taguchi method and Box-Benken design while the failure load were the output variables [21]. Effect of the face milling variables to surface roughness and the effect of roughness to the shear strength were studied in [22]. The CCD experiment and multi-objective optimization model was successfully implemented in the laser solder jet bonding process to determine the optimal process parameters [23]. The strength of adhesively bonded shear lap joint reinforced with multi-walled carbon nanotubes (MWCNT's) under different temperature was studied by utilizing the RSM [24]. The multiple linear regression and RSM to investigate the effect of the temperature, humidity, and specimen width was done by [25]. The failure mode was also observed to define the good conditions of peel test.

These literatures reveal that DOE is a good methodology which can be used in process optimization successfully. Most articles identify the key process parameters and then performs the experiment to obtain the regression model. This regression model will be solved by optimization approach to yield the optimal process conditions. Therefore, the purpose of this paper is to utilize the RSM to determine the optimal process

parameters that can maximize the shear strength of the adhesive joint for slider bonding process. The solution validation will be provided as well.

## 2. Materials and Methodology

### 2.1. Equipment and Materials

The slider boning is a process to join the slider to the suspension pad which is the dissimilar joint. The critical factors of this process must be investigated by the experiment based on the equipment and test procedure. The objective of this process optimization is to maximize the adhesive strength while preventing the thin suspension from damaging. The process flow of slider bonding process as in Fig. 2 comprises of: suspension loading, adhesive dispensing, slider bonding, UV curing, IR oven curing, and shear test.

The slider bonding requires automation system with high precision. Experiment investigation are performed with the slider bonding machine shown in Fig. 3(a) and 3 (b). The system installation consists of: (1) dispenser system by Nordson EFD-741 micro dot valve, (2) slider placing, (3) UV system of Hoya Execure 4000 with output intensity 4000 mW/cm<sup>2</sup> and wave length 300-400 nm, and (4) coordinated with the motion system via image processing and computer interface. The epoxy adhesive is dispensed onto suspension pad as depicted in Fig 1(a). The chemical composition of epoxy adhesive is given in Table 1. Epoxy adhesive between slider and suspension pad is pre-cured by UV and proceeded to IR oven (see Fig. 4) with temperature profile of 125 ± 10 °C for completely curing the adhesive. The HGA after adhesive curing process is depicted in Fig. 5.

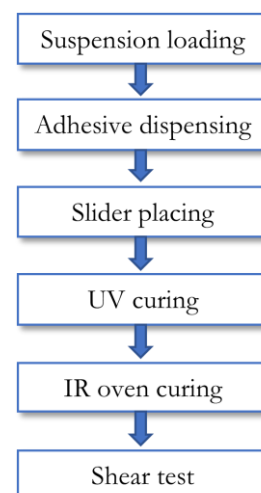
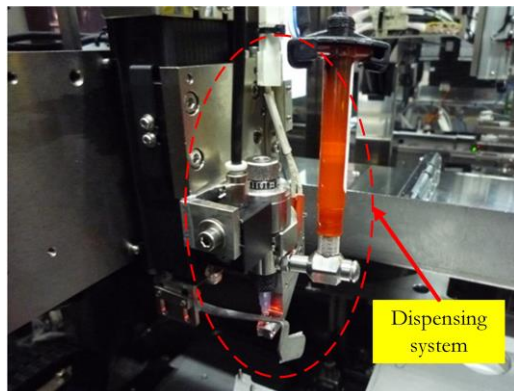


Fig. 2. Process flow of the slider bonding.

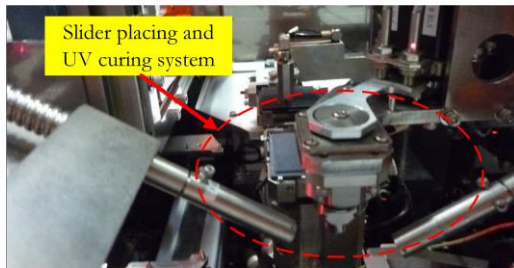
### 2.2. Shear Test for Epoxy Adhesive Joint

A major quality characteristic of slider is the adhesion force which is measured by the shear test equipment. Slider flies over the magnetic media disk with very narrow gap. When read and write mode, the slider almost touches

the magnetic disk. Therefore, the strength of slider is a vital quality which must be measured to ensure the product quality. The maximization of adhesive bonding is our primary objective. However, other quality aspects such as the epoxy fillet height and suspension damaging must be observed after curing process. The computer controller with force gage is used to measure the shear test for adhesive joint of HGA. All measurements are acquired using speed of 200  $\mu\text{m}/\text{min}$  and the load resolution of 0.001N. Figure 6 shows the shear test equipment used in this experiment. The maximum shear force in gram-force (gf) can be obtained from this shear equipment. The epoxy residual on the suspension pad and the backside of slider after shear test as in Fig. 7(a) and 7(b) indicate the correct failure mode of shear test for HGA.



(a)



(b)

Fig. 3. Slider bonding equipment. (a) the dispensing system (b) the slider placing and UV curing system.

Table 1. Chemical composition for epoxy adhesive.

| Element   | %Weight |
|---|---------|
| 3,4-Epoxy cyclohexylmethyl 3, 4-epoxycyclohexanecarboxylate (ECC) | 35%     |
| Resin Copolymers  | 50%     |
| Amorphous fumed silica  | 10%     |
| Butyrolactone   | 5%      |



Fig. 4. IR oven for completely curing the adhesive joint.

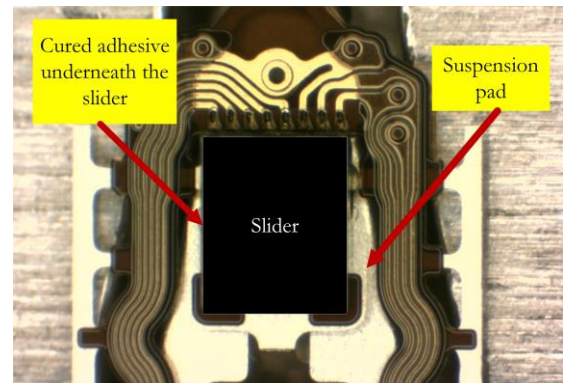


Fig. 5. Figure of HGA product after curing process.

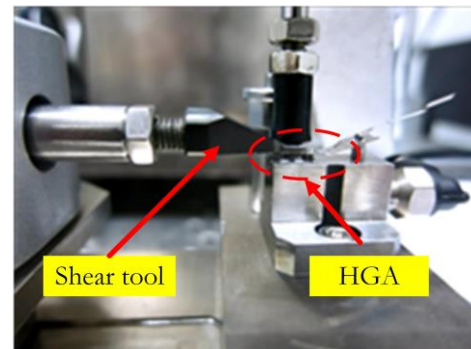
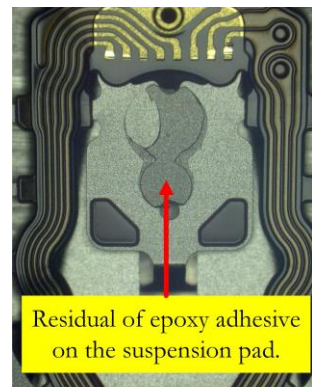
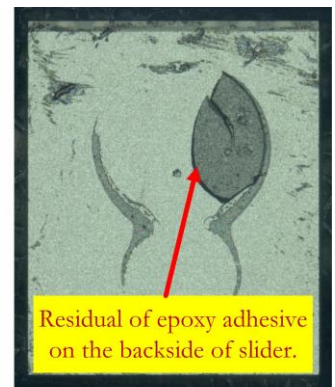


Fig. 6. Shear test equipment for the epoxy adhesive joint.



(a)



(b)

Fig. 7. (a) The residual of the epoxy adhesive on the suspension pad (b) the residual of the epoxy adhesive on the backside of slider.

### 2.3. Key Process Parameters for Slider Bonding Process

The shear strength of the adhesive joint depends up on the process parameters of the slider bonding process. There are three major process steps contribute to the shear strength of slider bonding process including dispensing process, slider placing, and adhesive curing by IR oven. Thus, the potential equipment setting, or process parameters employed to the experiment investigation can be listed as follows:

**Pressing distance (P):** Pressing distance is directly proportional to the force applied to adhesive under the slider during dispensing move down. This parameter affects the profile of adhesive under the slide on the suspension pad. High level of the pressing distance implies that high pressure is applied to both the epoxy resin and the suspension pad.

**Spring force (S):** Spring force is controlled as the spring back force for slider bonding process. It is a reaction force against the force from dispensing process. High level of spring force increases the force on slider placing process. Changing the spring force is obtained by adjusting the spring displacement in unit of  $\mu\text{m}$ .

**Holding time (H):** Holding time is used for controlling the spread of adhesive under slider. This parameter can affect the bond line thickness.

**Dot size (D):** Dot size of adhesive is a measure of the volume of adhesive dispensed onto the suspension as in Fig. 1. Improper amount of adhesive impacts the adhesion shear force.

**Curing time (C):** Curing time of IR oven needs to be controlled to achieve the complete curing of the adhesive.

The pressing distance, spring force, and holding time can contribute to the adhesive bond line thickness and the adhesive dispersion.

### 2.4. Response Surface Methodology

An importance procedure for this work is the experiment plan. The experiment is conducted by using the RSM. This work utilizes the central composite design for experiment plan. The CCD has the rotatability property. Rotatability is vital property for quadratic model so that the predictions will have a reasonable consistent and stable variance of the predicted response [26]. The design matrix for CCD consists of the factorial design points, axial design points and center points

In this experiment, the design matrix of CCD is based on five factors. The analysis of variance is performed to determine the significant terms in quadratic model. The coefficients of regression model reveal the relationship between the KPOV or response variable and process parameters (or KPIVs). Next, the optimization approach is then used to determine the optimal process conditions. The quadratic regression model can be written as in Eq. (1).

$$y = \beta_0 + \sum_{i \in K} \beta_i x_i + \sum_{\substack{i \in K \\ i < j}} \sum_{\substack{j \in K \\ i \neq j}} \beta_{ij} x_i x_j + \sum_{i \in K} \beta_{ii} x_i^2 + \varepsilon \quad (1)$$

where  $y$  is the response variable or observation value,  $x_i$  is the key process parameter  $i$ ,  $\beta_0$  is the constant term,  $\beta_i$  is coefficient of main effect,  $\beta_{ij}$  is coefficient of interactions,  $\beta_{ii}$  is the coefficient of quadratic terms,  $K$  is the number of factors in the experiment, and  $\varepsilon$  is the random error.

The fitted regression model for the predicted value of response variable, can be expressed in Eq. (2).

$$\hat{y} = X \hat{\beta} \quad (2)$$

where  $\hat{y}$  is the fitted value of the response variable,  $\hat{\beta}$  is the coefficient matrix, and  $X$  is the design matrix including constant column, main effects ( $x_i$ ) column, interaction effects ( $x_i x_j$ ) columns and quadratic terms ( $x_i^2$ ) column. The observation,  $y$ , obtained from the experiment design will be used in estimating the regression coefficients for the model as in Eq. (3).

$$\hat{\beta} = (X'X)^{-1} X'y \quad (3)$$

The experiment plan is designed based on the CCD. The levels of five factors are displayed in Table 2. This CCD requires 52 total runs including 32 factorial design points, 10 axial points, and 10 center points (shown in Table 3 and 4). The design matrix in uncoded-unit for factorial and center points are shown in Table 2. The response variable is the adhesive shear strength (gram-force). The axial points can be calculate using alpha ( $\alpha$ ) equals to 2.378. Thus, the axial points are extended beyond the factorial point by 2.378 times.

Table 2. Levels of factors of the factorial and center points for the CCD.

| Parameters            | unit          | Level |     |     |
|-----------------------|---------------|-------|-----|-----|
|                       |               | -1    | 0   | +1  |
| Pressing distance (P) | $\mu\text{m}$ | 50    | 75  | 100 |
| Spring force (S)      | $\mu\text{m}$ | 0     | 15  | 30  |
| Holding time (H)      | sec           | 2     | 3.5 | 5   |
| Dot Size (D)          | $\mu\text{m}$ | 200   | 225 | 250 |
| Curing time (C)       | min           | 12    | 16  | 20  |

## 3. Results and Discussion

### 3.1. Analysis of Variance for RSM

The experiment results for the CCD are shown in Table 3 and 4. The shear strength in gram-force is the response variable. The ANOVA as in Table 5 is utilized to identify the significant effects of the corresponding terms. The F distribution is used to test the hypothesis on the significant of terms in ANOVA. Any term having P-value

less than the significant level ( $\alpha = 0.05$ ) means that it has significant effect to the shear strength. For the hierarchical model, all lower-order terms that comprise the higher-order term also appear in the model. Table 5 displays the reduced model for the CCD. It is seen that the main effects, two-way interactions effects, and the quadratic effects are significant; therefore, the nonlinear relationship is presented.

The error term ( $\varepsilon$ ) of the ANOVA must be normally distributed. Therefore, the residuals which are the difference between the observation ( $y_i$ ) and the fitted value ( $\hat{y}_i$ ) are plotted on the normal probability plot as in Fig. 8. P-value of 0.204 for the normality test indicates that the residuals or errors of the experiment is normally distributed.

Table 3. Shear strength of the CCD for factorial points.

| Std. Order | P   | S  | H | D   | C  | Shear Strength (gf) |
|------------|-----|----|---|-----|----|---------------------|
| 1          | 50  | 0  | 2 | 200 | 12 | 182.5               |
| 2          | 100 | 0  | 2 | 200 | 12 | 202.5               |
| 3          | 50  | 30 | 2 | 200 | 12 | 180.1               |
| 4          | 100 | 30 | 2 | 200 | 12 | 186.9               |
| 5          | 50  | 0  | 5 | 200 | 12 | 188.9               |
| 6          | 100 | 0  | 5 | 200 | 12 | 191.5               |
| 7          | 50  | 30 | 5 | 200 | 12 | 186.2               |
| 8          | 100 | 30 | 5 | 200 | 12 | 183.8               |
| 9          | 50  | 0  | 2 | 250 | 12 | 191.6               |
| 10         | 100 | 0  | 2 | 250 | 12 | 196.8               |
| 11         | 50  | 30 | 2 | 250 | 12 | 190.5               |
| 12         | 100 | 30 | 2 | 250 | 12 | 186.1               |
| 13         | 50  | 0  | 5 | 250 | 12 | 181.1               |
| 14         | 100 | 0  | 5 | 250 | 12 | 182.5               |
| 15         | 50  | 30 | 5 | 250 | 12 | 191.2               |
| 16         | 100 | 30 | 5 | 250 | 12 | 179.1               |
| 17         | 50  | 0  | 2 | 200 | 20 | 172.0               |
| 18         | 100 | 0  | 2 | 200 | 20 | 199.8               |
| 19         | 50  | 30 | 2 | 200 | 20 | 165.6               |
| 20         | 100 | 30 | 2 | 200 | 20 | 182.4               |
| 21         | 50  | 0  | 5 | 200 | 20 | 180.9               |
| 22         | 100 | 0  | 5 | 200 | 20 | 189.8               |
| 23         | 50  | 30 | 5 | 200 | 20 | 173.6               |
| 24         | 100 | 30 | 5 | 200 | 20 | 180.6               |
| 25         | 50  | 0  | 2 | 250 | 20 | 168.4               |
| 26         | 100 | 0  | 2 | 250 | 20 | 194.7               |
| 27         | 50  | 30 | 2 | 250 | 20 | 175.3               |
| 28         | 100 | 30 | 2 | 250 | 20 | 180.2               |
| 29         | 50  | 0  | 5 | 250 | 20 | 167.6               |
| 30         | 100 | 0  | 5 | 250 | 20 | 182.2               |
| 31         | 50  | 30 | 5 | 250 | 20 | 171.5               |
| 32         | 100 | 30 | 5 | 250 | 20 | 176.5               |

The coefficient of the quadratic model can be obtained by using mathematical operation as given in Eq. (3). The coefficients of regression model in coded-unit variable are displayed in Table 6. The coded-unit regression model can be transformed to the uncoded-unit regression model as in Eq. (4).

$$\begin{aligned} \hat{y} = \text{Shear Strength} = & 160.7 + 0.777P - 0.833S \\ & + 10.26H + 0.2368D - 4.749C - 0.0071PS \\ & - 0.0653PH - 0.00233PD + 0.02944PC \\ & + 0.0544SH + 0.00452SD - 0.0462HD \\ & - 0.001592P^2 + 0.447H^2 + 0.05C^2 \end{aligned} \quad (4)$$

Table 4. Shear strength of the CCD for axial points and center points.

| Std. Order | P      | S      | H    | D      | C     | Shear Strength (gf) |
|------------|--------|--------|------|--------|-------|---------------------|
| 33         | 15.54  | 15     | 3.5  | 225    | 16    | 166.8               |
| 34         | 134.46 | 15     | 3.5  | 225    | 16    | 181.1               |
| 35         | 75     | -20.68 | 3.5  | 225    | 16    | 186.2               |
| 36         | 75     | 50.68  | 3.5  | 225    | 16    | 177.9               |
| 37         | 75     | 15     | 0.0  | 225    | 16    | 189.5               |
| 38         | 75     | 15     | 7.07 | 225    | 16    | 180.7               |
| 39         | 75     | 15     | 3.5  | 165.54 | 16    | 183.6               |
| 40         | 75     | 15     | 3.5  | 284.46 | 16    | 182.5               |
| 41         | 75     | 15     | 3.5  | 225    | 6.49  | 188.9               |
| 42         | 75     | 15     | 3.5  | 225    | 25.51 | 179.3               |
| 43         | 75     | 15     | 3.5  | 225    | 16    | 180.3               |
| 44         | 75     | 15     | 3.5  | 225    | 16    | 180.2               |
| 45         | 75     | 15     | 3.5  | 225    | 16    | 180.1               |
| 46         | 75     | 15     | 3.5  | 225    | 16    | 180.2               |
| 47         | 75     | 15     | 3.5  | 225    | 16    | 180.3               |
| 48         | 75     | 15     | 3.5  | 225    | 16    | 179.9               |
| 49         | 75     | 15     | 3.5  | 225    | 16    | 180.4               |
| 50         | 75     | 15     | 3.5  | 225    | 16    | 180.1               |
| 51         | 75     | 15     | 3.5  | 225    | 16    | 180.3               |
| 52         | 75     | 15     | 3.5  | 225    | 16    | 180.2               |

Table 5. ANOVA for the CCD experiment.

| Source         | DF | Adj SS  | Adj MS  | F-Value | P-Value |
|----------------|----|---------|---------|---------|---------|
| Model          | 15 | 2769.22 | 184.615 | 21.87   | <0.001  |
| P              | 1  | 608.99  | 608.986 | 72.15   | <0.001  |
| S              | 1  | 244.65  | 244.649 | 28.99   | <0.001  |
| H              | 1  | 112.86  | 112.861 | 13.37   | 0.001   |
| D              | 1  | 27.35   | 27.347  | 3.24    | 0.080   |
| C              | 1  | 613.71  | 613.712 | 72.71   | <0.001  |
| P <sup>2</sup> | 1  | 58.77   | 58.767  | 6.96    | 0.012   |
| H <sup>2</sup> | 1  | 58.02   | 58.021  | 6.87    | 0.013   |
| C <sup>2</sup> | 1  | 37.93   | 37.931  | 4.49    | 0.041   |
| P*S            | 1  | 226.85  | 226.845 | 26.88   | <0.001  |
| P*H            | 1  | 192.08  | 192.08  | 22.76   | <0.001  |
| P*D            | 1  | 67.86   | 67.861  | 8.04    | 0.007   |
| P*C            | 1  | 277.3   | 277.301 | 32.85   | <0.001  |
| S*H            | 1  | 48.02   | 48.02   | 5.69    | 0.022   |
| S*D            | 1  | 91.8    | 91.801  | 10.88   | 0.002   |
| H*D            | 1  | 95.91   | 95.911  | 11.36   | 0.002   |
| Error          | 36 | 303.85  | 8.44    |         |         |
| Total          | 51 | 3073.08 |         |         |         |

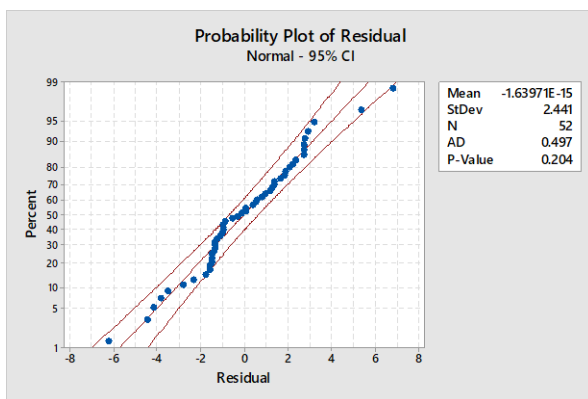


Fig. 8. Normal probability plot for the residual error.

### 3.2. Regression Model for RSM and Optimization

The coefficients of the quadratic regression equation reveals that all factors contribute to the shear strength. Due to the nonlinear relationship between key process parameters and the shear strength, the optimization approach is employed to determine the optimal process parameters under the range of factors in the design matrix.

The objective function for the optimization model is given in Eq. (5).

$$d = \begin{cases} 0 & ; \hat{y} < L \\ \left[ \frac{(\hat{y} - L)}{(T - L)} \right]^r & ; L \leq \hat{y} \leq T \\ 1 & ; \hat{y} > T \end{cases} \quad (5)$$

Table 6. Coefficients of the quadratic model in coded-unit.

| Term           | Coefficient | T-Value | P-Value |
|----------------|-------------|---------|---------|
| Constant       | 181.656     | 256     | <0.001  |
| P              | 3.75        | 8.49    | <0.001  |
| S              | -2.377      | -5.38   | <0.001  |
| H              | -1.618      | -3.66   | 0.001   |
| D              | -0.795      | -1.8    | 0.080   |
| C              | -3.765      | -8.53   | <0.001  |
| P <sup>2</sup> | -0.995      | -2.64   | 0.012   |
| H <sup>2</sup> | 1.005       | 2.62    | 0.013   |
| C <sup>2</sup> | 0.8         | 2.12    | 0.041   |
| P*S            | -2.662      | -5.18   | <0.001  |
| P*H            | -2.45       | -4.77   | <0.001  |
| P*D            | -1.456      | -2.84   | 0.007   |
| P*C            | 2.944       | 5.73    | <0.001  |
| S*H            | 1.225       | 2.39    | 0.022   |
| S*D            | 1.694       | 3.3     | 0.002   |
| H*D            | -1.731      | -3.37   | 0.002   |

where  $d$  is the desirability function for maximizing the objective,  $L$  is the lower bound for the fitted value of response variable ( $\hat{y}$ ),  $T$  is the target for the fitted value of response variable,  $r$  is the weight of desirability function, and  $\hat{y}$  is the fitted value of shear strength which is the response variable as in Eq. (4)

The mathematical model for optimization can be formulated as follows:

$$\text{Maximize } d = \begin{cases} 0 & ; \hat{y} < 200 \\ \left[ \frac{(\hat{y} - 200)}{(230 - 200)} \right]^r & ; 200 \leq \hat{y} \leq 230 \\ 1 & ; \hat{y} > 230 \end{cases} \quad (6)$$

Subject to

$$P \in [15.54, 134.46] \quad (7)$$

$$S \in [-20.68, 50.68] \quad (8)$$

$$H \in [0, 7.07] \quad (9)$$

$$D \in [165.54, 284.46] \quad (10)$$

$$C \in [6.49, 25.51] \quad (11)$$

The lower bound ( $L$ ) of 200 gf, the target ( $T$ ) of 230 gf, and the weight of desirability function ( $r$ ) of 1 are setup for the optimization model. The constraint (7) to (11) are the boundaries of factors based on the axial points of CCD as in Table 4. Next, this mathematical model is solved by the optimization engine in Minitab 17 and the optimal solution is shown in Table 7. The fitted value of 257.62 gf is the maximum shear strength under given constraints. The desirability equals to 1 that means the shear strength is greater than or equal to 230 gf. The 95% confidence interval for fitted mean is (240.06, 275.18) which means that the true mean of shear strength will be within this range with 95% confidence level.

Table 7. The optimal process parameters for the slider bonding process.

| Parameters            | Unit          | Setting |
|-----------------------|---------------|---------|
| Pressing distance (P) | $\mu\text{m}$ | 134.46  |
| Spring force (S)      | $\mu\text{m}$ | -20.68  |
| Holding time (H)      | sec           | 0       |
| Dot Size (D)          | $\mu\text{m}$ | 165.54  |
| Curing time (C)       | min           | 25.51   |

The surface plot displays the behavior of the response variable with respect to the key process inputs. Therefore, the surface plots shown in Fig. 9 to 12 are utilized to interpret the solution from the optimization. All surface plots present curvature effects of the quadratic model. It is seen that the shear strength of the optimal process parameters is at the peak of the surface plots. The shear strength is greater than the target of 230 gf which achieves the target of this optimization.

Highest pressing distance is required while the spring force at lowest level, the holding time of zero, and the dot size of 165.54  $\mu\text{m}$  is recommended to achieve the appropriate adhesive bond line. The UV curing time is applied with a few seconds and then proceed to the IR oven to perform the complete curing for 25.51 minutes.

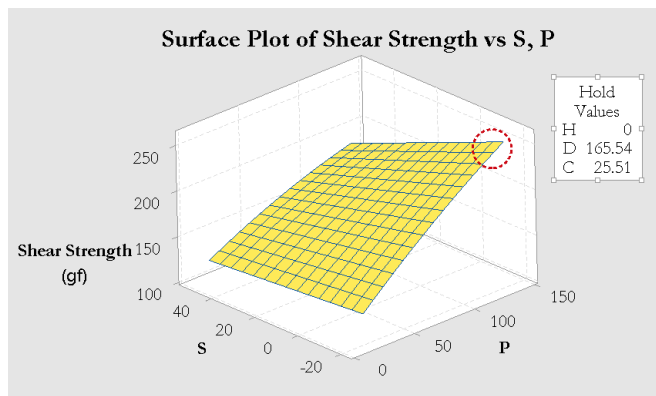


Fig. 9. Surface plot of the shear strength for P, S interaction.

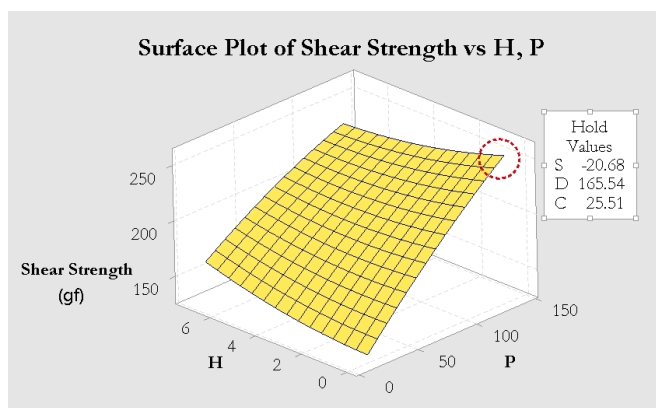


Fig. 10. Surface plot of the shear strength for P, H interaction.

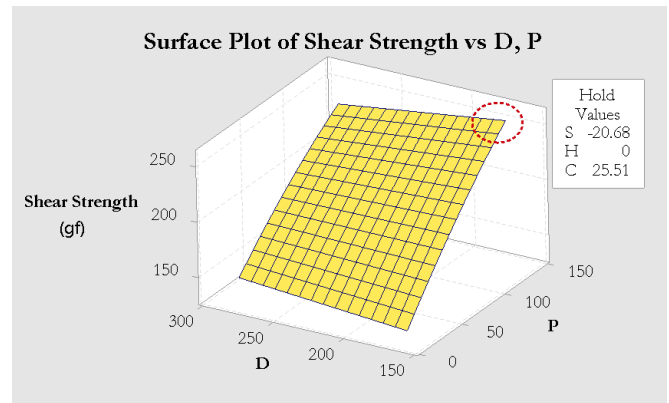


Fig. 11. Surface plot of the shear strength for P, D interaction.

The confirmation experiment is then conducted to validate the optimal process parameters. The slider bonding process is setup by using the parameters as in Table 7. Since the shear test is the destructive test, one unit of HGA per lot is tested. All data from 80 lots of HGA are sampled and plotted in the individual & moving range (I-MR) chart to validate the optimal process parameters (shown in Fig. 13). The mean shear strength of the confirmation runs is 253.51 gf fallen in the 95% confidence interval (240.06, 275.18) which is acceptable. The I-MR chart reveals that the shear strength is stable or within control. The prediction error of 1.6 % is accurate enough to be used as the prediction model for the slider bonding process.

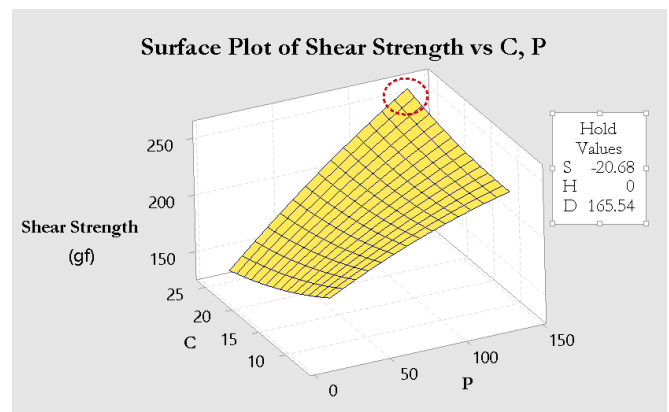


Fig. 12. Surface plot of the shear strength for P, C interaction.

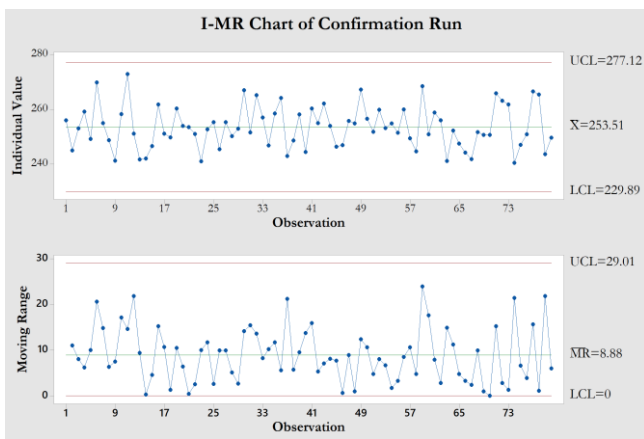
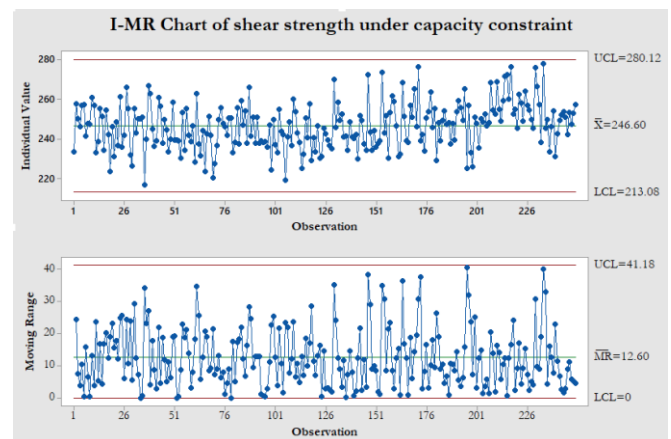


Fig. 13. I-MR chart for shear strength of confirmation run.

Fig. 14. I-MR chart for shear strength under capacity constraint ( $C = 20$  min.).

### 3.3. Prediction of the Shear Strength under Production Constraint

The quadratic regression mode can be used to predict the optimal shear strength under the production constraints. For HGA production line, there are more than two models operated in an assembly line. Therefore, a capacity constraint must be considered because it affects the output of the assembly line. In this case, the curing time of 20 minutes for IR oven is required to increase the line capacity and to satisfy the customer demand. The mathematical model as in Eq. (6) – (11) is solved by adding a constraint which is  $C = 20$  min. The optimal process parameter is then obtained as in Table 8. The fitted shear strength of 249.44 gf is obtained. This parameter is implemented with 250 lots to validate the accuracy of the prediction model. The I-MR chart of the shear strength for these 250 lots is depicted in Fig. 14 with the mean of 246.6 gf. It is found that the error of mean prediction is only 1.14%.

Table 8. The optimal process parameters for the slider bonding process when  $C = 20$  min.

| Parameters            | Unit          | Setting |
|-----------------------|---------------|---------|
| Pressing distance (P) | $\mu\text{m}$ | 134.46  |
| Spring force (S)      | $\mu\text{m}$ | -20.68  |
| Holding time (H)      | sec           | 0       |
| Dot Size (D)          | $\mu\text{m}$ | 165.54  |
| Curing time (C)       | min           | 20      |

### 4. Conclusion

The design of experiment using the RSM and the optimization approach are employed to perform an improvement on the shear strength of adhesive joint. Five key process parameters are investigated to identify their effects to the shear strength. These process parameters relate to: the force applying to the epoxy adhesive and the suspension, the amount of epoxy adhesive, and the curing time. The CCD experiment are performed and yield the appropriate quadratic regression model. The results of the CCD experiment show that all factors significantly contribute to the shear strength of the adhesive joint. The surface plots also confirm that the optimal process parameters can yield the maximum shear strength under the design boundary.

The confirmation experiment is performed to validate the results from the CCD. The I-MR chart is employed to observe the mean and stability of the shear strength for the slider bonding process. The result from confirmation experiment can confirm that the regression equation can provide the good prediction of the shear strength and the optimal process parameters can be used for the process control of slider bonding process. The prediction error of 1.6% also confirms that the regression model is capable for predicting the shear strength. This regression model is utilized to predict the shear strength when the curing time is reduced to 20 minutes in order to increase capacity of the assembly line. The error of mean prediction is only 1.14% reveals that the quadratic model obtained from the CCD experiment can be successfully used for controlling the slider bonding process when the process parameters need to be changed.

In summary, the results of this study mainly contribute the process improvement of the slider bonding process for HGA product. The optimal process parameters benefit to the process control of the HGA assembly process. The quality and reliability of HGA is increased due to the maximum shear strength is achieved by applying this approach.

## Acknowledgement

This research was supported by the Research and Researcher for Industry (RRI) under the Thailand Research Fund (TRF). It offers a scholarship for Ph.D. students at King Mongkut's University of Technology North Bangkok (KMUTNB) through grant PHD57I0070.

## References

- [1] I. Barboutis and V. Kamperidou, "Shear strength of beech wood joints bonded with commercially produced PVAc D3 adhesives," *Int. J. Adhes. Adhes.*, vol. 105, p. 102774, 2021.
- [2] L. Guo, J. Liu, H. Xia, X. Li, X. Zhang, and H. Yang, "Effects of surface treatment and adhesive thickness on the shear strength of precision bonded joints," *Polym. Test.*, vol. 94, p. 107063, 2021.
- [3] L. R. Bhagavathi, A. P. Deshoande, G. D. J. Ram, and S. K. Panigrahi, "Effect of cellulosic fillers addition on curing and adhesion strength of moisture-curing one-component polyurethane adhesives," *Int. J. Adhes. Adhes.*, vol. 108, p. 102871, 2021.
- [4] C. Zhang, L. Chen, G. Wang, J. Jin, and Y. Zhang, "Effects of laser processing crater array microstructure on the surface characteristics and bonding strength of Ti6Al4V adhesive joints," *Opt. Laser Technol.*, vol. 141, p. 107125, 2021.
- [5] P. A. M. G. P. Bamberg, U. Reisgen, A. Schiebahn, J. D. V. Barbosa, B. Marx, and R. S. Coelho, "Digital image correlation analysis of the effects of the overlap length, adhesive thickness and adherends yield strength over similar and dissimilar joints of high strength steel and aluminum alloys," *Int. J. Adhes. Adhes.*, vol. 83, pp. 69-75, 2018.
- [6] B. Schneider, V. C. Beber, J. Schweer, M. Brede, and B. Mayer, "An experimental investigation of the fatigue damage behaviour of adhesively bonded joints under the combined effect of variable amplitude stress and temperature variation," *Int. J. Adhes. Adhes.*, vol. 83, pp. 41-49, 2018.
- [7] L. Sun, Y. Tie, Y. Hou, X. Lu, and C. Li, "Prediction of failure behavior of adhesively bonded CFRP scarf joints using a cohesive zone model," *Eng. Fract. Mech.*, vol. 228, p. 106897, 2020.
- [8] B. R. Mose, I. S. Son, and D. K. Shin, "Adhesion strength of die attach film for thin electronic package at elevated temperature," *Microelectron. Reliab.*, vol. 91, pp. 15-22, 2018.
- [9] Y. Guan, X. Chen, F. Li, and H. Gao, "Study on the curing process and shearing tests of die attachment by Ag-epoxy electrically conductive adhesive," *Int. J. Adhes. Adhes.*, vol. 30, pp. 80-88, 2010.
- [10] H. Shi and T. Ueda, "Comparative studies on solder joint reliability of CTBGA assemblies with various adhesives using the array-based package shear test," *Microelectron. Reliab.*, vol. 51, pp. 1898-1902, 2011.
- [11] R. Sahin and S. Akpinar, "The effects of adherend thickness on the fatigue strength of adhesively bonded single-lap joints," *Int. J. Adhes. Adhes.*, vol. 107, p. 102845, 2021.
- [12] P. Hu, X. Han, W. D. Li, L. Li, and Q. Shao, "Research on the static strength performance of adhesive single lap joints subjected to extreme temperature environment for automotive industry," *Int. J. Adhes. Adhes.*, vol. 41, pp. 119-126, 2013.
- [13] G. Chen, L. Yu, Y. H. Mei, X. Li, X. Chen, and G. Q. Lu, "Reliability comparison between SAC305 joint and sintered nanosilver joint at high temperatures for power electronic packaging," *J. Mater. Process. Technol.*, vol. 214, pp. 1900-1908, 2014.
- [14] C. A. Yang, C. R. Kao, and H. Nishikawa, "Development of die attachment technology for power ic module by introducing indium into sintered nano-silver joint," in *IEEE 67th Electronic Components and Technology Conference (ECTC)*, 2017, pp. 1974-1980.
- [15] S. A. Bello, "Flex Performances of Epoxy Aluminium Particulate Composites," *Eng. J.*, vol. 22, no. 4, pp. 97-107, Jul. 2018.
- [16] L. S. Sutherland, C. Amado, and C. G. Soares, "Statistical analyses of the effects of bonding parameters and fabrication robustness on the strength of adhesive T-joints," *Compos. B. Eng.*, vol. 175, p. 107063, 2019.
- [17] M. A. A. Dzul-Cervantes, O. F. Pacheco-Salazar, L. A. Can-Herrera, M. V. Monerno-Chulim, J. I. Cauich-Cupul, P. J. Herrera-Franco, and A. Valadez-González, "Effect of moisture content and carbon fiber surface treatments on the interfacial shear strength of a thermoplastic-modified epoxy resin composites," *J. Mater. Res. Technol.*, vol. 9, pp. 15739-15749, 2020.
- [18] K. Khaothong, "Analysis of Failing load and optimization of hot air welding parameters on PVC-acrylic coated polyester fabric by Taguchi and ANOVA technique," *Eng. J.*, vol. 23, no. 6, pp. 331-344, Nov. 2019.
- [19] H. C. Cheng, K. Y. Hsieh, and K. M. Chen, "Thermal-mechanical optimization of a novel nanocomposite-film typed flip chip technology," *Microelectron. Reliab.*, vol. 51, pp. 826-836, 2011.
- [20] T. Sangsawang, N. Rongrat, and A. Yothayuth., "Optimization for Biodiesel Production by Transesterification with Electric Fields," *Eng. J.*, vol. 25, no. 2, pp. 261-268, Feb. 2021.
- [21] M. H. Kim, H. S. Hong, and Y. C. Kim, "Determination of failure envelope of functionally graded adhesive bonded joints by using mixed mode continuum damage model and response surface method", *Int. J. Adhes. Adhes.*, vol. 106, p. 102815, 2021.
- [22] S. Liu, S. Jin, X. Zhang, K. Chen, L. Wang, and H. Zhao, "Optimization of 3D surface roughness induced by milling operation for adhesive-sealing," *Procedia CIRP*, vol. 71, pp. 279-284, 2018.

- [23] J. Deeying, K. Asawarungsaengkul, and P. Chutima, "Multi-objective optimization on laser solder jet bonding process in head gimbal assembly using the response surface methodology," *Opt. Laser Technol.*, vol. 98, pp. 158-168, 2018.
- [24] H. Khoramishad, R. S. Ashofteh, M. Mobasheri, and F. Berto, "Temperature dependence of the shear strength in adhesively bonded joints reinforced with multi-walled carbon nanotubes," *Eng. Fract. Mech.*, vol. 199, pp. 179-187, 2018.
- [25] I. Amatya, J. Seo, T. Letcher, and J. H. Ahn, "Peel and cleavage strength tests with adhesive connections in dynamic message signs," *Int. J. Adhes. Adhes.*, vol. 103, p. 102715, 2020.
- [26] D. C. Montgomery, "Response surface methods and designs," in *Design and Analysis of Experiments*, 8th ed. New York: John Wiley, 2012, pp. 478-500.



**Santi Pumkrachang** is a PhD candidate in the Faculty of Engineering, King Mongkut's University of Technology North Bangkok, Thailand. He has experience in the hard disk drive industry for 24 years. His experience and the area of interests include the improvement on the manufacturing and assembly process in hard disk drive assembly, process optimization, assembly process development, measurement system, tool design, fixture design, and automation process.



**Krisada Asawarungsaengkul** graduated in Production Engineering from King Mongkut's University of Technology North Bangkok and took his Master's degree from Chulalongkorn University. He received his PhD degree in Industrial Engineering from Sirindhorn International Institute of Technology, Thammasat University. Currently, he is an Associate Professor in the Faculty of Engineering at King Mongkut's University of Technology North Bangkok, Thailand. His research interests include lean six sigma, optimisation in operations and manufacturing system, improvement on the electronic assembly manufacturing, advanced quality control, and smart factory technology. He has involved in the industrial research projects. He has published several articles in refereed journals and conference proceedings.



**Parames Chutima** received his Engineering degree from Chulalongkorn University. He received his Master's degree from Chulalongkorn University and Asian Institute of Technology. He received his PhD degree in Manufacturing Engineering and Operations Management from the University of Nottingham. Currently, he is a Professor in the Faculty of Engineering at Chulalongkorn University, Bangkok, Thailand. His research interests include multi-objective optimisation in operations management, production planning and control of assembly lines, just-in-time production systems and simulation modelling. He is the author of several international publications in conference proceedings and referred journals.